IEEE Access
Multidisciplinary ⋮ Rapid Review ⋮ Open Access Journal

Received 3 April 2024, accepted 8 April 2024, date of publication 15 April 2024, date of current version 23 April 2024.

Digital Object Identifier 10.1109/ACCESS.2024.3388913

RESEARCH ARTICLE

Variational Mode Decomposition and Empirical Wavelet Transform-Based Feature Extraction and Ensemble Classifier for Lower Limb Movement Prediction With Surface Electromyography Signal

GUNDALA JHANSI RANI[1], (Member, IEEE), MOHAMMAD FARUKH HASHMI[1], (Senior Member, IEEE), AND GHULAM MUHAMMAD[2], (Senior Member, IEEE)

[1]Department of Electronics and Communication Engineering, National Institute of Technology, Warangal 506004, India
[2]Department of Computer Engineering, College of Computer and Information Sciences, King Saud University, Riyadh 11421, Saudi Arabia

Corresponding author: Ghulam Muhammad (ghulam@ksu.edu.sa)

This work was supported by the Researchers Supporting Project, King Saud University, Riyadh, Saudi Arabia, under Grant RSP2024R34.

ABSTRACT Surface Electromyography (sEMG) signal classification and analysis have attracted particular attention because of their many biological applications. These can be utilized for kinesiological research, motion intention recognition, human-machine interaction, rehabilitation, and disease diagnosis. Due to the interference of noise, these signals are challenging to process. To attenuate noise interference from sEMG signals, a denoising method based on Variational Mode Decomposition (VMD) with selected Intrinsic Mode Functions (IMFs) based on Correlation Coefficient (CC) and Empirical Wavelet Transform (EWT) is proposed in this study. The suggested method applies the EWT to the specific IMFs obtained by VMD, decomposing the raw signal with noise into several IMFs based on correlation coefficients. To increase the signal separability, stability and to extract the low-frequency information of the signal, apply EWT on selected IMFs; it decomposes IMFs into the multiresolution analysis (MRA). Following segmentation, 16 Features are recovered using the time domain, frequency domain, and entropy with an overlapping window technique of 250ms and 50% overlap. Later, four machine learning classifiers— Linear Discriminant Analysis (LDA), Support Vector Machine (SVM), Naive Bayes (NB), and Ensemble Subspace k-nearest Neighbor (KNN) — are used to identify the three lower limb movements. The results obtained for an Ensemble Subspace KNN classifier have a 98.9% accuracy, a 98.8% F1-Score, and a 98.7% sensitivity. Lastly, machine learning (ML) is used in this work to create a new feature extraction technique for lower limb activity prediction based on VMD-EWT with CC.

INDEX TERMS Electromyography (EMG), variational mode decomposition (VMD), empirical wavelet transform (EWT), machine learning (ML).

I. INTRODUCTION

Lower limb activity recognition (LLAR) has gained significance due to its practicality in several domains, such as monitoring the health of the elderly, surveillance and security systems, detecting human falls, and numerous more applications [1], [2]. Surface electromyography signals (sEMG), being a kind of neurological signals, are often used in many healthcare applications [3], such as controlling prosthetics or exoskeletons, evaluating neuromuscular diseases, monitoring physical activity, and numerous others [4].

The associate editor coordinating the review of this manuscript and approving it for publication was Sotirios Goudos.

Motion recognition and estimation have been extensively researched utilizing a variety of sensors and wearable devices. Researchers have concentrated on the upper limb applications of sEMG signals since acquiring sEMG signals from muscles in the lower limbs is more challenging because muscles interact with multiple motor units simultaneously. This contrasts lower-limb applications, which have received less attention from scientists. Recognizing gait activities from a lower limb's surface electromyographic signal is crucial for controlling an exoskeleton for a person with knee deformities or a prosthesis for someone unable to walk due to amputation. The authors in [5] proposed a neural network-based approach to sEMG signal classification for myopathy and neuropathy. By examining sEMG signals, Rezaee and coworkers [6] could diagnose Parkinson's disease. Shukla et al. [7] looked into using ML classifiers to label six different kinetic actions of the lower extremities. Data from healthy and unhealthy persons with uneven surface EMG signals due to different-sized signal durations was collected to aid in diagnosing knee abnormalities [8]. Both healthy and unwell people contributed to this data set. After multiple procedures were employed to perform multistep classification, a computational classifier offered final recognition. Gautam and coworkers developed a novel classification method [9] to forecast the angle at which the knee will bend. A convolutional neural network (CNN) extracted features from the sEMG signal data. For joint angle prediction, a long short-term memory (LSTM) network was used, and a follow-up dense layer was coupled to interpret the features and classify them. CNN and LSTM form the architecture used to categorize lower limb actions. The sEMG signal data was processed using CNN to extract features. The sEMG signal's frequency can be anything from 10 to 500 Hz, and its amplitude can be anything from 0 to 10 mV [10]. Various filters can exclude noises too high or too low for the sEMG signals to detect. These filters include band-pass, high-pass, and low-pass filters, among others. However, they cannot filter out inactive sEMG signal spectrum band noises like white Gaussian noise. They have this restriction on their abilities. Reference [11] declare that the Wigner-Ville distribution (WVD) technique can be used to describe the frequency ranges of the motor unit in a sEMG signal.

Empirical mode decomposition (EMD) is a method presented for signal decomposition [12]. The authors in [13] state that one advantage of EMD is to make no assumptions about the data and that the signal is always represented in the time domain. Conversely, wavelet-based denoising methods analyze the signal in the frequency domain after transforming it there [46]. Most of these algorithms cannot function because they assume the data to be static. Stochastic and non-stationary best define the characteristics of EMG signals. To enhance the quality of the input signal, denoising algorithms based on EMD have been proposed. Intrinsic Mode Functions (IMF) were extracted from the input signal via EMD's recursive recognition of local extrema values. Using these estimates and some interpolation, this can determine the signal's upper and lower envelopes [14]. The high-frequency components or oscillations are effectively segregated by employing an average of envelopes as the low-pass centerline. The primary drawbacks of EMD-based denoising schemes are intermingling intermodal frequencies (IMFs) and relying on various interpolation and extrema detection techniques for decomposition [13]. These limitations lead to a high sensitivity of the EMD to sampling and noise. Several EMD variations have been proposed as possible answers to the mode mixing issue, and the inclusion of ensemble empirical mode decomposition (EEMD) has been documented [15]. The authors conducted a comprehensive ensemble empirical mode decomposition (CEEMD) [16]. To remedy the situation, several EMD versions were created. The algorithmic framework employed in this research is the Empirical Modal Decomposition Class (EMDC) [17] technique. Nevertheless, the predominant focus of current research has revolved around using a solitary EMDC technique to estimate energy consumption in buildings. Power line interference (PLI), white Gaussian noise (WGN), and baseline wandering (BW) are the primary causes of noise in EMG signals [18]. Furthermore, modifications and enhancements have been made to technologies such as variational mode decomposition (VMD) and empirical wavelet transform (EWT) to tackle the previously identified challenges associated with EMDC. The decomposition approaches employed in this study do not offer a comprehensive resolution to the mode-mixing problem and result in a significant computational burden during implementation [16]. The VMD was developed by Dragomiretskiy et al. by extending the Wiener filter into multiple adaptive bands [19]. The VMD is an inherent, highly flexible method for decomposing signals into their respective variational mode functions (VMF). Every VMF recovered after demodulation was found to be perfectly smooth and have its core frequency. VMD obtains the individual VMF components about the signal's frequency domain to avoid mode mixing. Applications of VMD-based denoising include seismic time-frequency analysis, bearing fault diagnostics identification, wind speed forecasting, and denoising biological imaging [20]. da Silva et al. [42] developed the Berg Balance Scale (BBS) score prediction utilizing electromyographic and dynamometric data. The goal is to determine which variables most predict geriatric fall risk and how they relate to muscle groups. Gupta et al. [43] proposed classification algorithm and dual-stage FSA. Single-muscle approaches perform worse than dual-muscle approaches, with Linear Discriminant Analysis, Neural Network, and Support Vector Machine classifiers performing best, on the other hand, the EMD method is vulnerable to noise and sampling errors. There is no supporting mathematical theory, and there may be considerable overlap in the frequency ranges of the individual components. Due to these constraints, the signal will be denoised inadequately, with some noise signals still present in the processed signals [21]. Jérôme Gilles developed the EWT [21] to solve these problems with the EMD method, inspired by the fact that EMD

is similar to an adaptive filter bank. As a result of its valuable qualities, EWT has attracted a lot of attention and has been used in various fields, including fault diagnosis [22], [23]. Li et al. [41] worked on Ship-radiated noise (SN) marine signal, but contamination hindered feature extraction. This paper proposes SVMD, FuDE, and wavelet packet denoising. SN is adaptively classified as signal, noise-signal, and noise intrinsic mode functions (IMFs). Reconstructing signal and noise-signal IMFs produce a denoised signal. Chen et al. [44] propose an enhanced long-term usability and user adaptation of the surface electromyography-based pattern recognition system (sEMG-PRS) by the use of a stacked weighted random forest (SWRF) algorithm, which addresses the imbalanced performance of single-channel surface electromyography (sEMG) data for lower limb movement identification. Wei et al. [40] worked on entropy information with the signal's variational modal functions (VMF). The approach was evaluated on four lower limb movements from twenty people and exhibited 95.82% and 97.44% accuracy for two muscles. Gupta et al. [37] projected that neuromuscular problem diagnosis and kinesiological research require surface EMG (sEMG) signals employing hybrid wavelet-ensemble empirical mode decomposition (WD-EEMD). Lower extremity exoskeleton robots can be more lifelike using a wavelet packet transform-based sliding window difference average filtering feature extract algorithm and UKFNN identification algorithm. SEMG energy feature models improve neural network weights and decrease noise. Lower limb motion intention recognition studies outperform BPNN with an average accuracy of 94.83%. New and trustworthy, the method works. Wavelet packet transform-based sliding window difference average filtering feature extract and unscented Kalman neural network (UKFNN) identification algorithms by Shi et al. [45] improve lower extremities exoskeleton robot practicality. Lower limb motion intention recognition experiments demonstrate an average accuracy of 94.83%, exceeding the backpropagation neural network (BPNN) technique. From the above literature the existing decomposition models suffer from several shortcomings, including the absence of mathematical modelling, inadequate backward error correction, ineffective noise handling, rigid band limits in wavelet transform, and the requirement to set filter bank boundaries prior to implementing EWT to overcome this limitation,this research proposes an improved EMG signal preprocessing with hybrid method, feature set combination, and ensemble classifiers for lower limb movement prediction.

The proposed work makes significant contributions in the following areas:

1) Determining an individual's lower limb activity from the sEMG signals derived from their leg muscles.

2) Proposed VMD-EWT (Variational Mode Decomposition —Empirical Wavelet Transform),as a hybrid pre-processing method for analyzing sEMG signals to identify lower limb activity.

3) A total of sixteen features were extracted using the overlapping window approach, including time domain, frequency domain, and entropy measures.

4) The Ensemble Subspace KNN performance parameters were computed, assessed, and contrasted with earlier research to identify lower limb activity in healthy participants.

The paper will follow the structure described below. Section II discusses the dataset; in Section III, the proposed methodology with a block diagram, VMD, EWT, segmentation, feature extraction, ML models used, and performance evaluation analysis is discussed in detail. In Section IV, the results and discussion are provided. The conclusion and future scope are provided in Section V.

II. DATASET DESCRIPTION

The researchers obtained data from the publicly accessible original electromyography (EMG) dataset, which was last updated on May 30, 2023, from PLOS ONE [24]. The initial electromyography (EMG) dataset consisted of recordings from the vastus medialis muscle in the specified leg of 14 individuals in good health participating in three distinct training regimens. These regimens included activities such as gait (walking), leg flexion (standing), and leg extension from a seated position (sitting).

As part of the EMG data collection protocol, a single electrode was strategically placed on the vastus medialis muscle group, while a goniometer was positioned on the knee joint. The Datalog device MWX8 (http://www.biometricsltd.com/datalog.htm) was utilized to collect EMG data, featuring eight digital channels and four analog channels. One digital channel monitored and recorded EMG signals, while another tracked goniometry data of the knee joint of the detected foot. The data, sampled at a frequency of one kilohertz, were stored internally on the MWX8 device and transmitted via the real-time Datalog program using the Bluetooth adapter for offline analysis.

The participants underwent three separate workout programs targeting the knee joint, involving leg flexion while standing, leg extension while sitting, and walking. EMG signals originating from the vastus medialis muscle of the identified leg were observed and documented. Participant ages ranged from 28 to 7.82 years, heights from 174 to 5.88 centimeters, and weights from 67.64 to 11.35 kilograms.Two experimental sessions were scheduled, comprising standing-sitting and walking exercises. Participants performed these programs randomly for both sessions, commencing with a tone-paced timing of one second with one-second intervals, followed by a five-second rest interval. Each motion was executed five times to mitigate potential intra-subject variability.

III. PROPOSED METHODOLOGY

The procedure of the proposed lower limb activity recognition method is depicted in FIGURE 1. The raw EMG dataset was obtained from the public domain. The EMG signal was

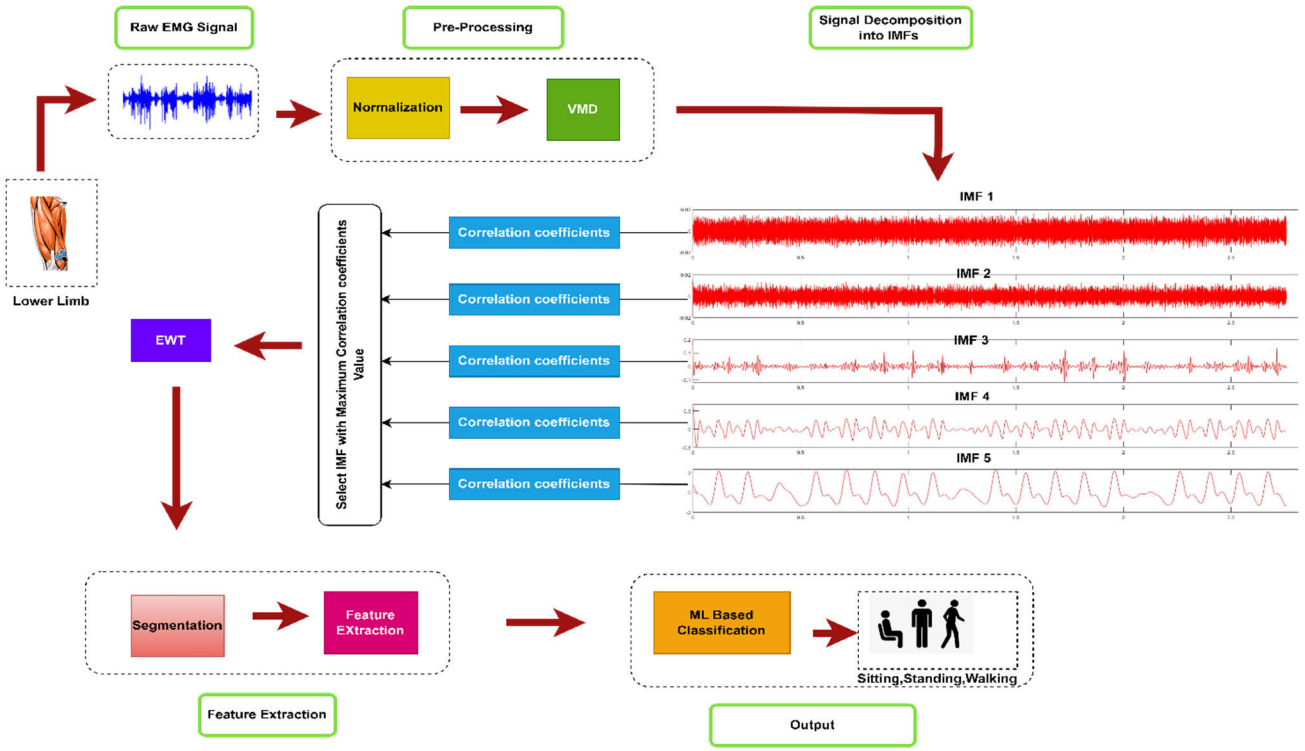

FIGURE 1. Block diagram for the proposed methodology.

first preprocessed using VMD to get rid of background noise, and then the data was split into five independent motion fields (IMFs). Selected IMFs underwent EWT after being determined using correlation coefficients. Statistical analysis was utilized to choose Time-domain, Frequency-domain, and entropy features from each MRA that showed statistically significant differences in three lower limb motions, and these were then combined to form a new feature vector. Three different lower-body motions were categorized using the multi-class classifier. Possible applications of the proposed method include exoskeleton control, rehabilitation training, and monitoring of regular activities. In addition, Algorithm 1 gives the pseudocode for the suggested procedure, which is included below. The procedure and experiment are laid out in full below.

A. DATA NORMALIZATION

The sEMG signals underwent preprocessing before the classification task. The EMG signals were first processed using Z-Score standard normalization, and VMD denoising was later applied to normalized data. Equation 1 illustrates the normalization of a channel's Z-Score [29].

$$F(x_t) = \frac{x_t - \mu}{\sigma} \tag{1}$$

where x_t denotes the sEMG signal, μ denotes its mean value and σ standard deviation, respectively.

Algorithm 1 Pseudocode of the Proposed Method

1. Input: sEMG signal S = $[s_1, s_2, s_3, \ldots\ldots, s_{14}]$, where s_i denotes the sEMG signal recorded by the ith sEMG sensor for three activities: walking, sitting, standing (i = 1, 2, 3, …, 14)
2. Preprocessing
Apply Active Normalization to preprocess the sEMG signal recorded data.
3. Denoising with VMD
for j = 1 to 5 do # Number of IMF's obtained by decomposing the sEMG signal with VMD
Perform VMD decomposition on sEMG signal
for j = 1 to 5 do # IMF's obtained from VMD decomposition
Compute correlation coefficients for each IMF
Select Max correlation coefficient value among IMF's
if correla > 0.3 then
Apply Empirical Wavelet Transform (EWT)
4. Segmentation
Segment each EWT-transformed IMF (X(j)) into 250ms window size with 50% overlap
Applied for each sample of lower limb movement of each subject
5. Feature Extraction
Extract 16 features from each segmented window
6. Machine Learning Classification
Feed the 16 extracted features into four machine-learning models
Apply 5-fold cross-validation for model evaluation
7. Output: Recognition accuracy (Accuracy(j))

B. SEMG DECOMPOSED WITH VMD

Adaptive signal processing is done using the VMD approach. In addition to efficiently breaking down both high- and

low-frequency signals to lessen nonlinearity, smoothness, and time series complexity, VMD [20] also fixes issues with mode size and endpoint confusion with the EMD. The method for formulating and resolving the functional analysis variational problem forms the foundation of VMD. The following symbols are used to identify FM (amplitude-modulated-frequency-modulated) signals, also referred to as IMFs:

$$IMF_n(t) = A_n(t)cos(\phi_n(t)) \tag{2}$$

where, $A_n(t)$ is the amplitude envelop, $\phi_n(t)$ is the phase of the signal.

Additionally, two conditions must be fulfilled for the IMFs of VMD:

(1) Each IMF's center frequency bandwidth sum is minimized;

(2) The total of all IMFs equals the original signal.

The following optimization issues can be created from the decomposition procedure using VMD, presuming that each mode component's frequency, u_k, is concentrated close to a center frequency ω_k, during the decomposition process. Optimization aims to find k modes with the minimum combined bandwidth for all modes. It should also be confirmed that the sum of all methods equals the initial signal $f(t)$. The following is one way to turn the optimization problem into a variational problem, as shown in Equation 2

$$\begin{aligned} &\min_{\{u_k\},\{\omega_k\}} \left\{ \sum_{k=1}^{k} \left\| \partial_t \left[(\delta(t) + j/\pi t) * u_k(t) \right] (e^{-(j\omega_k t)} \right\|_2^2 \right\} \\ &s.t. \sum_{k=1}^{k} u_k = f(t) \end{aligned} \tag{3}$$

where u_k and ω_k denote the kth mode and corresponding center frequency of the mode, respectively, and f (t) represents the initial input signal, δ(t) represents the Dirac distribution function, t represents time, and "$*$" symbolizes the convolution process. The letters $\{u_k\}$ stand for the set of modes $\{u_1, u_2, \ldots, u_k\}$, $\{\omega_k\}$ denotes the set of center frequencies $\{\omega_1, \omega_2, \ldots .\omega_k\}$ .k is the overall number of modes. FIGURE 3 illustrates the VMD flow chart to execute the VMD model on data.

The quadratic penalty term and the Lagrangian penalty operator are employed to solve equation 3 to obtain the optimal solution. The inclusion of a quadratic penalty term serves to mitigate the influence of noise on the decomposition of the signal, while the introduction of the Lagrangian penalty operator ensures the preservation of the constraints. Together, these two changes enable the ideal solution to be found.

$$\begin{aligned} &L(\{u_k\}, \{\omega_k\}, \lambda) \\ &= \alpha \sum_{k=1}^{k} \left\| \partial_t \left[\left(\delta(t) + {}^{j}/_{\pi t} \right) * u_k(t) \right] e^{-(j\omega_k t)} \right\|_2^2 \\ &\quad + \left\| f(t) - \sum_{k=1}^{k} u_k(t) \right\|_2^2 \\ &\quad + \left\langle \lambda(t), f(t) - \left| \sum_{k=1}^{k} u_k(t) \right\rangle \right. \end{aligned} \tag{4}$$

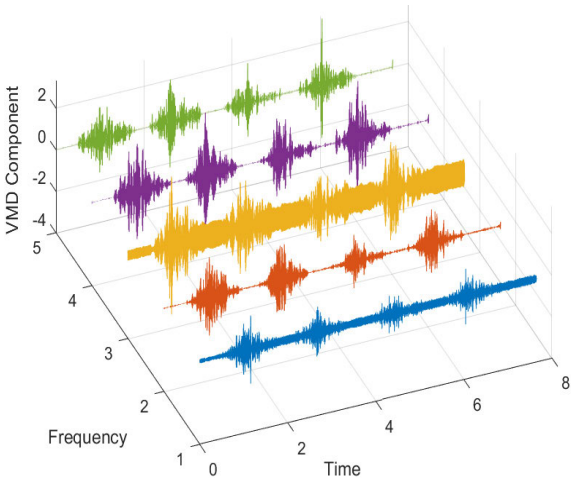

FIGURE 2. 3D visualization of IMFs obtained from VMD.

where λ (t) is the Lagrange multiplier, and α is the regularization factor, $\left\| f(t) - \sum_{k=1}^{k} u_k(t) \right\|_2^2$ is a quadratic penalty term.

To solve the overall optimization problem, the alternate direction method of multipliers (ADMM) is utilized. This method provides a solution by treating the issue as a succession of iterative sub-optimization problems, as demonstrated by equation 4. These subproblems aim to continually find the lowest possible value for the cost function associated with the parameter of interest [30].

$$\hat{u}_k^{n+1}(\omega) = \frac{f(\omega) - \sum_{i \neq k} \hat{u}_i(\omega) + \frac{\hat{\lambda}(\omega)}{2}}{1 + 2\alpha(\omega - \omega_k)^2} \tag{5}$$

$$\omega_k^{n+1} = \frac{\int_0^\infty \omega \left| \hat{u}_k(\omega) \right|^2 d\omega}{\int_0^\infty \left| \hat{u}_k(\omega) \right|^2 d\omega} \tag{6}$$

$$\hat{\lambda}^{n+1}(\omega) \leftarrow \hat{\lambda}^n(\omega) + \tau((\hat{f}(\omega) - \sum_k \hat{u}_k^{n+1}(\omega)) \tag{7}$$

where τ is the parameter of noise tolerance, and n represents the current number of iterations.

The following is the convergence condition of the above equation when solving VMD:

$$\frac{\sum_{k=1}^{M} \left\| \hat{u}_k^{n+1} - \hat{u}_k^n \right\|_2^2}{\left\| \hat{u}_k^n \right\|_2^2} < \varepsilon \tag{8}$$

where $\varepsilon > 0$ is the given discriminant accuracy.

The obtained five IMFs can be visualized in FIGURE 2, where normalized data is applied with VMD. The extracted IMFs' 3D visualization is shown below.

Ultimately, f(t) yields K narrow-band IMF components, $u_k(t)$, which can be stated as follows.

$$f(t) = \sum_{k=1}^{k} u_k(t) \tag{9}$$

where K is the quantity of extracted IMFs. The common consensus is that the IMF component has more noise the lower the correlation coefficient [31] between the IMF Component

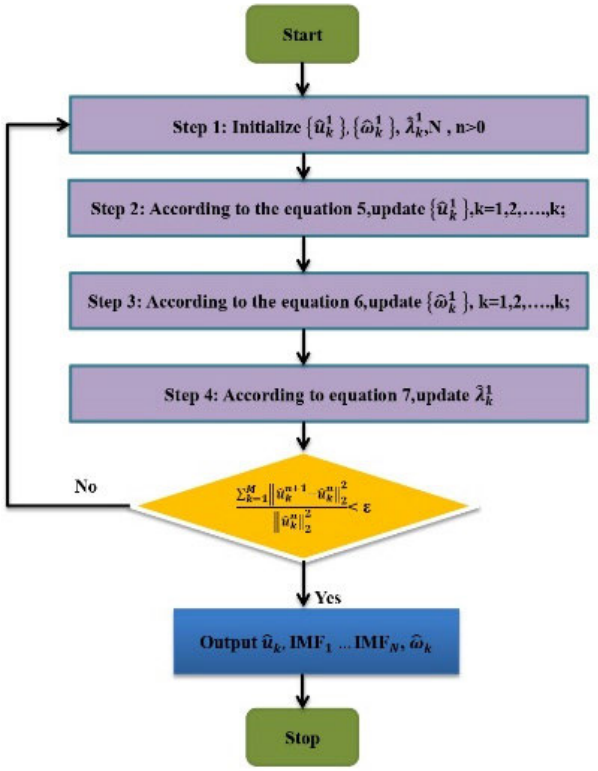

FIGURE 3. Flowchart of VMD.

and the decomposed signal. As a result, it determined the correlation coefficients between each decomposed sEMG signal f(t) and its corresponding IMF component $u_k(t)$. It is known to include the greatest noise because the high-frequency component IMF1 $u_1(t)$ with the highest center frequency and its decomposed sEMG signal f(t) have the lowest correlation coefficient, which is often below 0.3, which is weakly correlated. Contemplating highly linked IMFs discovered using VMD. The correlation coefficients between the original signal and the five IMFs acquired by VMD are shown in TABLE 1. IMF3, IMF4, and IMF5 have higher correlation coefficients, while IMF1, IMF2, and channel 1 and channel 2 have lower correlation coefficients. For every subject, correlation coefficients were also computed. Chosen the highest IMF values for the subsequent procedure and FIGURE 3 illustrate the flowchart of VMD.

C. APPLY EWT ON SELECTED IMFS

This research suggests using information on lower limb motion characteristics to gather more comprehensive data. Selected IMFs from VMD were processed using EWT. Empirical wavelet transform (EWT) is a method for adaptive signal decomposition [21]. To divide the original signal into numerous low-power sub-signals with a small support spectrum of Fourier, EWT creates a segmentation of the Fourier spectrum of the original signal using a bank of wavelet filters.

The following are the main steps in an empirical wavelet transform:

TABLE 1. Correlation coefficient values obtained from subject 1 while performing gait, sitting, and standing activities during VMD with 5 IMFs.

IMFs	Correlation Coefficients					
	Gait		Sitting		Standing	
	Channel 1	Channel 2	Channel 1	Channel 2	Channel 1	Channel 2
IMF 1	0.276	0.00012	0.080	0.0025	0.225	0.0004
IMF 2	0.432	0.0007	0.218	0.0237	0.411	0.0007
IMF 3	0.671	0.0013	0.406	0.081	0.667	0.001
IMF 4	0.601	0.155	0.616	0.490	0.574	0.147
IMF 5	0.482	0.999	0.793	0.984	0.505	0.999

First, the Selected IMF's Fourier spectrum is separated into N continuous pieces.

The second step involves building a band-pass filter using an empirical wavelet. In each segment, the empirical scaling functions ϕn(ω) and wavelet functions ψn(ω) are defined as follows:

$$\varphi_n(\omega) = \begin{cases} 1, |\omega| \le (1-\varsigma)\omega_n \\ \cos[\frac{\pi}{2}\beta(\frac{1}{2\varsigma\omega_{n+1}}(|\omega| - (1-\varsigma)\omega_n)] \\ (1-\varsigma)\,\omega_n \le |\omega| \le (1+\varsigma)\,\omega_n \\ 0, otherwise \end{cases} \tag{10}$$

$$\psi_n(\omega) = \begin{cases} 1, (1+\varsigma)\,\omega_n \le |\omega| \le (1-\varsigma)\,\omega_{n+1} \\ \cos[\frac{\pi}{2}\beta(\frac{1}{2\varsigma\omega_{n+1}}(|\omega| - (1-\varsigma)\,\omega_{n+1}] \\ (1-\varsigma)\,\omega_n \le |\omega| \le (1+\varsigma)\,\omega_{n+1} \\ \sin[\frac{\pi}{2}\beta(\frac{1}{2\varsigma\omega_n}(|\omega| - (1-\varsigma)\,\omega_n] \\ (1-\varsigma)\,\omega_n \le |\omega| \le (1+\varsigma)\,\omega_n \\ 0, otherwise \end{cases} \tag{11}$$

where the function $\beta(x)$ is defined ad:

$$\beta(x) = \begin{cases} 0, & x \le 0 \\ x^4\left(35 - 84x + 70x^2 - 20x^3\right), & 0 < x < 1 \\ 1, & x \ge 1 \end{cases} \tag{12}$$

The following ζ gives the description of the limiting condition of the parameter that must be met to ensure that empirical scaling functions ϕn(ω) and wavelet functions ψn(ω), have tight frames:

$$\zeta < \min(\frac{\omega_{n+1} - \omega_n}{\omega_{n+1} + \omega_n}) \tag{13}$$

The third step is calculating both the approximation and the details of the coefficients. The approximate coefficient W_f (0, t) may be obtained by taking the inner product of

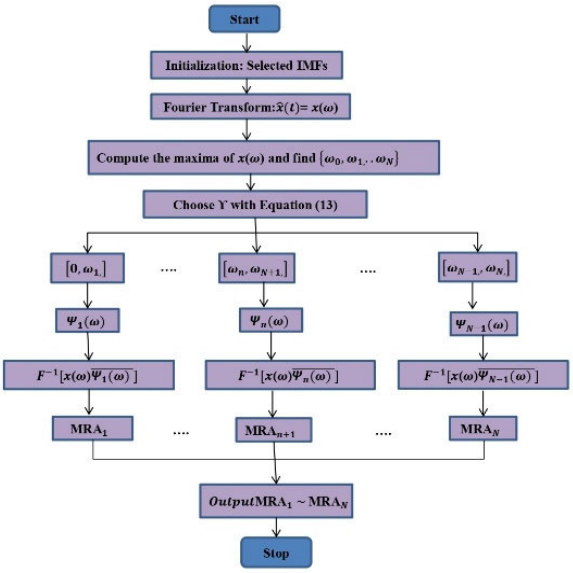

FIGURE 4. EWT Flowchart.

the original signal and the empirical scaling function f(τ). On the other hand, the detail coefficients W_f(n, t) can be obtained by taking the inner product of the original signal and the empirical wavelets function. The following are the expressions that can be used:

$$W_f\ (0, \mathrm{t}) = \int \mathrm{f}(\tau)\overline{\varphi_1(\tau - t)d\tau} \tag{14}$$

$$W_f(n, t) = \int \mathrm{f}(\tau)\overline{\psi_n(\tau - t)d\tau} \tag{15}$$

$\psi_n(\tau - \mathrm{t})$ and $\varphi_1(\tau - \mathrm{t})$ denote the conjugate of complex numbers

Fourth step: Perform the calculations needed to determine the sub-signals, often known as empirical mode functions. The following are some possible definitions for the first sub-signal $f_1(t)$ and the nth sub-signal $f_n(t)$

$$f_1(t) = W_f\ (0, \mathrm{t}) * \varphi_1(t) \tag{16}$$

$$f_n(t) = W_f(n, t) * \psi_n(t) \tag{17}$$

where $f_1(t)$ and $f_n(t)$ each represent the first sub-signal and the n^{th} sub-signal respectively, where $*$ represents the convolution process of numbers $\psi_n(\tau - \mathrm{t})$ and $\varphi_1(\tau - \mathrm{t})$) or correlation coefficients for every subject in the study. The maximum possible values for the IMFs are selected for use in the next procedure. The step-by-step evaluation process for EWT can be seen in FIGURE 4.

D. SEGMENTATION

The EMG signals have a random quality to them. Because of the randomness, an EMG signal needs to be segmented. The segmentation of EMG signals has been accomplished by applying the windowing technique [32]. EMG data can be segmented using either an overlapping or an adjacent windowing technique (FIGURE 5). In this study, overlapping windowing was utilized with a window length of 256 milliseconds and a percentage of overlap of fifty percent [33].

TABLE 2. Time domain feature set F1:.

S. No	ExtractedTime Domain Feature	Mathematical Formulation
1	Mean Absolute Value	$MAV(x) = \frac{1}{L}\sum_{k=1}^{L}\lvert x_k\rvert$ *Where x_k is a sample of the sEMG signal*
2	Root Mean Square	$RMS = \sqrt{\frac{1}{L}\sum_{k=1}^{L}\lvert x_k\rvert^2}$
3	Zero Crossing	$ZC = \sum_{k}^{L-1} f(x_k)$ Where $f(x_k) = \begin{cases} 1 & if\ , x_k > 0\ and\ x_{k+1} < 0 \\ & or\ x\_k < 0\ and\ x\_(k+1) > \\ 0 & otherwise \end{cases}$
4	Kurtosis	$Kurt = \frac{E[(x-\mu)^4]}{\sigma^4}$
5	Skewness	$Skew = \frac{E[(x-\mu)^3]}{\sigma^3}$ *where μ = Mean of the dataset, E is the Expected value estimator of the dataset, and σ is the standard deviation of the signal dataset,*
6	Standard Deviation	$STD(x) = \frac{\sum_{K=0}^{L-1}(x_k - \bar{x})^2}{L-1}$

E. FEATURE EXTRACTION

After the sEMG signals have been pre-processed and segmented, the next step, feature extraction, focuses on the relevant structures within the signals. When choosing features, ensure they compress the right data and separate the output classes as much as possible. The F1-Time Domain Features, F2-Frequency Domain Features, and F3-Entropy Features are computed using 16 features. TABLE 2, TABLE 3, and TABLE 4 illustrate the extracted features with their mathematical formulation.

The Extracted features are given to machine learning classifiers, where F4 gives the best results compared to other feature sets, as shown in FIGURE 5. Summarized feature vector can be observed in TABLE 5, where F4 gives the highest accuracy compared with F1, F2, and F3. When VMD is applied on dataset F4 achieves good results -NB-52%, SVM-85.5%, LDA-82.7%, and ensemble subspace KNN-96.4%. Similarly, when EWT is applied to the dataset, F4 gives the best result -NB-59.9%, SVM-90.1%, LDA-82.8%, and ensemble subspace KNN-98.8%. Finally, when we applied VMD-EWT, the results obtained were NB-59.9%, SVM-93.9%, LDA-83.5%, and ensemble subspace KNN-99.3%.

F. MACHINE LEARNING MODELS

The proposed model is evaluated using machine learning classifiers such as LDA, SVM, NB, and ensemble subspace KNN. This study used surface electromyography (sEMG)

TABLE 3. Frequency domain feature set F2:.

S.No	Extracted Frequency Domain Feature	Mathematical Formulation
1	Mean frequency	$MNF = \sum_{j=1}^{M} f_j p_j / \sum_{j=1}^{M} p_j$ where fj is the frequency of the spectrum at frequency bin j, Pj is the EMG power spectrum at frequency bin j, and M is the length of the frequency bin.
2	Median frequency	$MDF = \frac{1}{2}\sum_{j=1}^{M} p_j$ MDF is a frequency at which the spectrum is divided into two regions with equal amplitude
3	Band Power	BP = Σ(P(f) * df) for f in [f_low, f_high]; power spectral density P(f) of the signal for each frequency bin within the desired band (from f_low to f_high)

TABLE 4. Entropy feature set F3:.

S.No	Extracted Entropy Feature	Mathematical Formulation
1	Permutation Entropy	$PermEn = \sum_{i=1}^{N} p_i log_2(p_i)$
2	Distribution Entropy	$DistEn = \frac{-1}{log_2(N)} \sum_{i=1}^{N} p_i log_2(p_i)$ where $the\ p_i$-product of the probability of each data point
3	Spectral Entropy	$SpecEn = -\sum_{i=1}^{N} \frac{p_i log_2(p_i)}{log_2 N}$
4	Dispersion Entropy	$DispEn = \sum_{\Pi=1}^{e^n} p(\Pi_{u_0 u_1 \ldots\ldots u_{n-1}} . \ln(\Pi_{u_0 u_1 \ldots\ldots u_{n-1}}))$
5	Phase Entropy	$PhasEn = \frac{-1}{\log(N)} \sum_{j=1}^{N} p(j) log_2(p(j))$;p(j)=$\frac{S_\theta[j]}{\sum_{j=1}^{n} S_\theta[j]}$

F4 =F1+F2+F3(Combination of all features)

data to classify three lower limb activities using machine learning classifiers. Classifications were successful.

1) SUPPORT VECTOR MACHINE (SVM)

The SVM, a supervised machine learning classifier, boasts versatility through its utilization of various kernels, enabling it to tackle both linear and non-linear classification tasks proficiently. This versatility empowers SVM to address a wide range of classification problems, regardless of their linear or non-linear nature, simultaneously and effectively [25].

2) LINEAR DISCRIMINANT ANALYSIS (LDA)

The LDA is an instrument that has proven effective within machine learning. It is well-known for its expertise in dimensionality reduction and classification efforts, which are significant research fields, and it has won numerous awards for its work in these areas.

LDA [26] maps high-dimensional data to low-dimensional space, which makes it simpler to discern between the many types of groups. The concept behind this method is to achieve the greatest possible inter-class separation while simultaneously reducing the amount of variance within each class as much as possible. In circumstances involving more than one class, LDA is very helpful since the linear transformation enables the classifier to make intelligent decisions based on a determined decision boundary. Its ability to increase class separability, as well as the fundamental principles that it is based on, gives it significance in a wide variety of applications, which is the primary reason for its importance.

3) NAIVE BAYES (NB)

In probabilistic machine learning, the Naive Bayes classifier [27] is a tried-and-true algorithm that finds broad use in many classification endeavors. The aforementioned

TABLE 5. Summarized feature vector (F1,F2,F3 and F4) with VMD,EWT and VMD-EWT with ML classifiers.

Methods	Feature Vector	Classifier Accuracy (%)			
		NB	SVM	LDA	Ensemble Subspace KNN
VMD	F1	49.7	58.4	61.6	89.6
	F2	41.2	49.1	55.0	91.1
	F3	51.0	80.3	67.8	92.3
	F4	**52.0**	**85.5**	**82.7**	**96.4**
EWT	F1	58.4	59.6	54.1	86.3
	F2	58.7	70.6	61.9	98.5
	F3	56.1	85.8	76.7	96.5
	F4	**59.9**	**90.1**	**82.8**	**98.8**
VMD-EWT	F1	64.6	73.0	68.7	89.1
	F2	67.6	69.8	70.0	98.9
	F3	65.6	83.3	78.6	96.3
	F4	**68.7**	**93.9**	**83.5**	**99.3**

(Best values found are in bold)

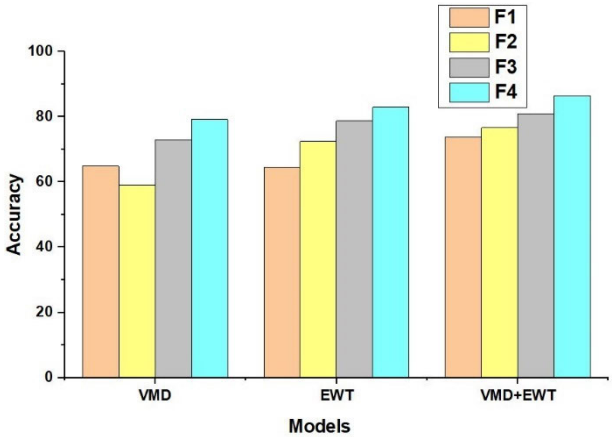

FIGURE 5. Accuracy comparison for various features F1 -Time Domain feature set, F2-Frequenct Domain Feature set,F3-Entropy Feature set and F4 - combined features of F1,F2,F3.

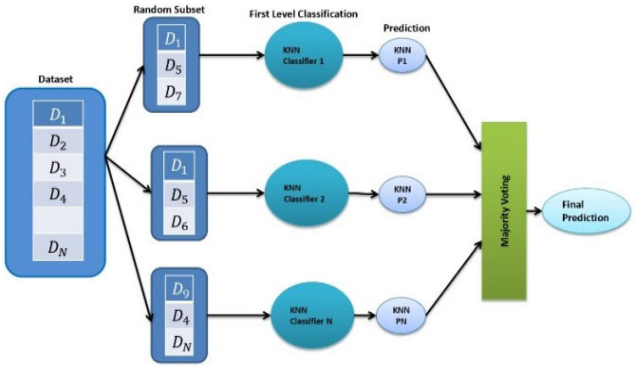

FIGURE 6. Ensemble subspace KNN mode.

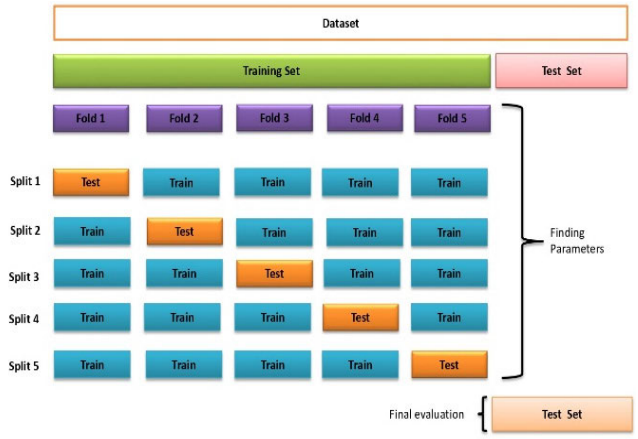

FIGURE 7. A visual representation of the 5 × 5 fold cross-validation.

researchers developed it. It has been demonstrated to be successful in several settings, although it appears quite straightforward. Bayes' theorem is the basis for the classifier, which bases its forecasts on the probabilistic connections between the various features and categories. Because it operates under the assumption that the attributes are conditionally independent, it performs admirably with both small and large datasets. This ensures the calculations are easy to understand while enhancing the algorithm's overall performance. Naive Bayes classifiers excel in various applications, including text classification, spam filtering, sentiment analysis, and other jobs that satisfy the conditional independence assumption satisfactorily. Naive Bayes is a suitable choice for classification jobs that need to be done quickly and accurately, even though its assumption does not always hold in practice.

4) ENSEMBLE SUBSPACE KNN

Within the framework of subspace k-NN, three of the most influential theories in machine learning are brought together [28]. Through the utilization of ensemble learning, the power of multiple models may be merged, which ultimately results in a more accurate forecasting system. On the other hand, subspace learning emphasizes dimensionality reduction while concurrently retaining essential data properties. This is accomplished without sacrificing any of the properties of the data. The last method, k-NN, is straightforward and creates predictions according to the group that makes up most of the k's nearest neighbors. When these two concepts are combined, the complex solution utilizes reduced-dimensional data representations in conjunction with the k-NN methodology. This approach can improve classification difficulties in terms of both their accuracy and their generalizability. The subspace k-NN algorithm combines three significant facets of machine learning when used to classify individuals. To begin, the ensemble methodology capitalizes on the combined predictive capacity of several diverse models, increasing performance when taken as a whole. Second, subspace learning reduces the number of dimensions that make up the input while preserving the data deemed the most crucial. The simplicity of the k-NN approach, which is based on the closeness of neighboring nodes, contributes to the overall result. There are more important factors than this, though. This combination produces a sophisticated approach that combines the k-NN classification process with lower-dimensional data representations. This combination also gives a refined method. It holds the potential for better accuracy and efficiency, especially in situations requiring complicated classification, as shown in FIGURE 6.

G. PERFORMANCE EVALUATION ANALYSIS

Accuracy, Precision, F1-Score, and Sensitivity serve as performance measurements of lower limb activity recognition. It is important to calculate the true positive rate, the false positive rate, the true negative rate, and the false negative rate to assess the performance of machine learning models. The conclusions of these estimations aid in the creation of confusion measures.

In this particular investigation, each column of matrix C represents the percentage of examples in each anticipated class, and each row indicates the percentage of instances in each actual class or vice versa. The walking (G), sitting (S), and standing (D) categories can be used to describe the results of this study, specifically utilizing the matrix.

$$C = \begin{bmatrix} C_{GG} & C_{GS} & C_{GD} \\ C_{SG} & C_{SS} & C_{SD} \\ C_{DG} & C_{DS} & C_{DD} \end{bmatrix} \tag{18}$$

where C_{GG} is the number of walking class instances anticipated to walk, C_{GS} *is* the number of walking class instances anticipated to sitting,

C_{GD} is the number of walking class instances anticipated to stand, and to the same extent, others can be defined.

Total number of data points (T)= $C_{GG} + C_{GS} + C_{GD} + C_{SG} + C_{SS} + C_{SD} + C_{DG} + C_{DS} + C_{DD}$

Total number of cases as predicted walking $(P_G) = C_{GG} + C_{SG} + C_{DG}$

Total number of cases as actual walking $(A_G) = C_{GG} + C_{GS} + C_{GD}$

Total number of cases as predicted sitting $(P_S) = C_{GS} + C_{SS} + C_{DS}$

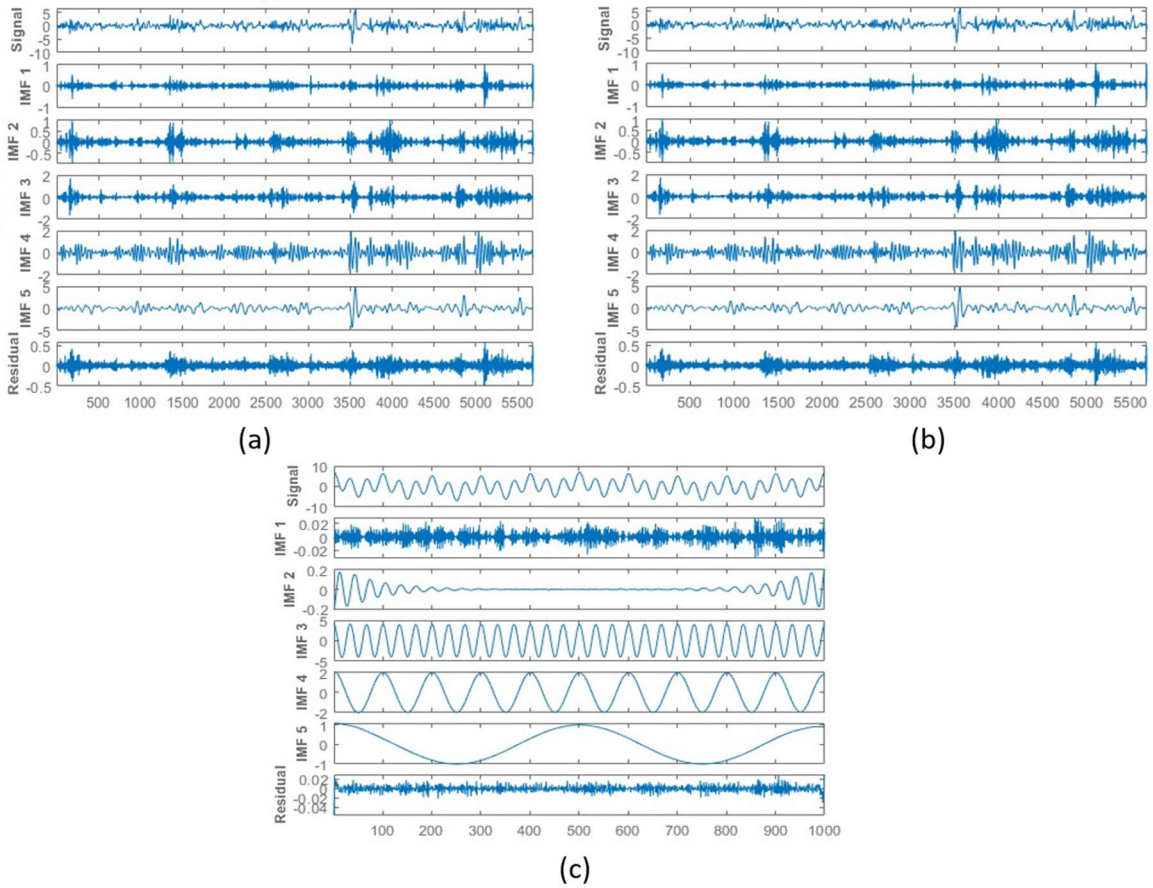

FIGURE 8. A Sample of EMG Signal and IMFs: a)Walking b)Sitting c)Standing.

Total number of cases as actual sitting $(A_S) = C_{SG} + C_{SS} + C_{SD}$

Total number of cases as predicted standing $(P_D) = C_{GD} + C_{SD} + C_{DD}$

Total number of cases as actual standing $(A_D) = C_{DG} + C_{DS} + C_{DD}$

The performance parameters for three class datasets:

Accuracy- refers to a measurement that determines how correct an overall categorization model is. It works out the percentage of total instances that have been accurately predicted relative to the total number of instances.

$$\text{Accuracy} = \frac{C_{GG}+C_{SS}+C_{DD}}{T} * 100 \tag{19}$$

Precision- When comparing all of the model's positive predictions, precision is the percentage of true positive predictions. Other names for it include the Positive Predictive Value.

$$Precision\,(PR_i) = \frac{C_{ii}}{P_i} * 100 \tag{20}$$

Sensitivity (Recall)- The amount of true positive predictions made out of the total number of actual positive cases is what sensitivity assesses. It quantitatively measures the model's capacity to detect positive events accurately.

$$Sensitivity(RC_i) = \frac{C_{ii}}{A_i} * 100 \tag{21}$$

F1-Score- The harmonic mean of recall and precision is known as the F1-Score. It offers a fair assessment that accounts for both false positives and false negatives.

$$F1 - Score = 2 * \frac{(Precision * sensitivity)}{(Precision + sensitivity)} \tag{22}$$

where i ϵ {G,S,D}

IV. RESULT AND DISCUSSIONS

This study predicates classifying lower limb motion with sEMG data using VMD-EWT. Using a dataset of 14 healthy persons performing three different activities (walking, sitting, and standing), an experimental evaluation of the proposed method for recognizing lower limb activities based on surface electromyography (sEMG) signals was conducted. This was done on the MATLAB-R2022a version to experimentally evaluate the proposed strategy for recognizing lower limb activities. Using VMD-EWT, in this study, the individuals' activity signals were pre-processed and the data were split into training and testing sets using the 5-fold cross-validation method. For signal decomposition, an overlapping window

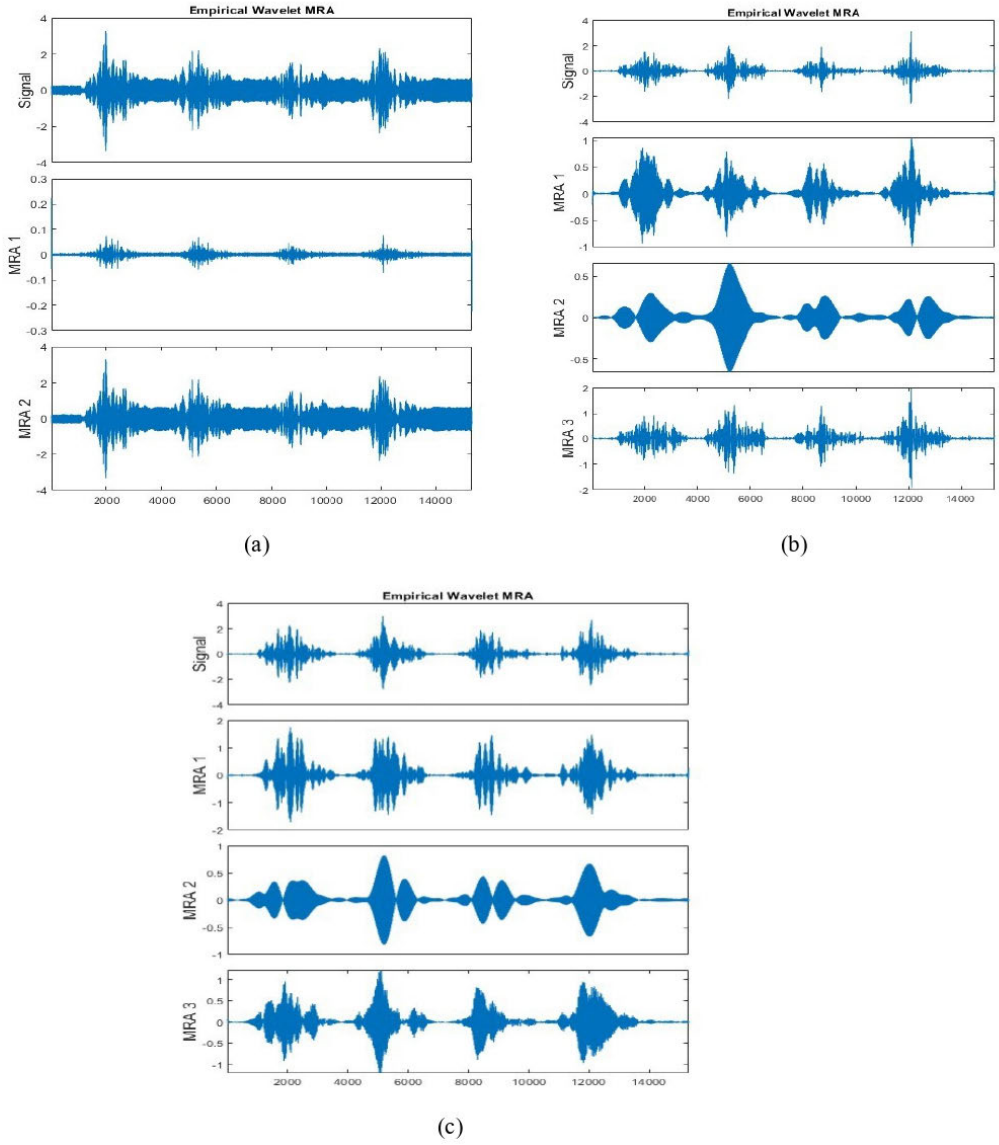

FIGURE 9. EWT on selected (a) IMF3, (b) IMF4, (c) IMF5 for subject1 during walking.

with a size of 250ms and a 50% overlap was employed. Subsequently, machine learning techniques were utilized to extract features and label the outcomes. Classifiers such as Linear Discriminant Analysis, Naive Bayes, Support Vector Machine, and Ensemble Subspace KNN were employed.

The K-fold cross-validation approach is a resampling procedure that examines the efficacy of AI models by employing a coercive information test. This evaluation is carried out by dividing the data into K-folds. In the context of this methodology, the samples are divided into groups of k different sizes that are all the same, as seen in FIGURE 7. After that, the model is trained using k groups of samples and then validated using k groups of samples. Both of these steps are repeated until the model is complete. This procedure is repeated for each group based on the initial data. The findings proved that utilizing the proposed Ensemble Subspace KNN classifier in conjunction with the VMD-EWT preprocessing method effectively achieved the desired results. This combination achieved a remarkable accuracy of 98.9% when recognizing the three movements of the lower limbs, which is a significant accomplishment. The accuracy and precision metrics were validated by a battery of experiments, which provide solid proof of the method's practicability and potential utility in a wide range of circumstances that can be found in the real world. The fact that the proposed strategy could generate such a high level of accuracy in the classification of lower limb activities is evidence of the method's dependability in the domain of sEMG signal processing.

Two different preprocessing approaches, VMD and EWT, collaborated to efficiently extract relevant features

TABLE 6. Subject-wise validation accuracy was obtained using VMD, EWT, VMD-EWT with four different classifiers- Naïve Bayes,SVM, LDA, and ensemble subspace KNN classifier with the 5-fold cross validation technique for human activity prediction during sitting, standing and walking.

Subject	VMD				EWT				VMD-EWT			
	NB	SVM	LDA	Ensemble Subspace KNN	NB	SVM	LDA	Ensemble Subspace KNN	NB	SVM	LDA	Ensemble Subspace KNN
S1	73.6	81.3	78.6	88.8	84.8	85.9	92.9	84.4	52.9	83.4	73.3	**97.2**
S2	68.5	81.5	80.7	88.9	86.2	88.1	92.6	83.8	53.9	88.8	78.9	**97.7**
S3	64.8	90.7	85.9	95.4	59.8	86.0	93.5	96.5	75.3	93.2	83.1	**99.6**
S4	55.2	81.1	78.0	96.0	78.5	84.0	95.2	98.9	83.8	88.1	90.6	**99.6**
S5	61.5	85.7	81.7	97.7	84.0	85.0	97.3	99.5	54.2	89.4	86.4	**98.6**
S6	72.9	93.1	89.5	93.1	76.2	87.6	95.5	99.5	83.2	89.9	87.5	**96.6**
S7	61.7	98.4	97.4	98.4	72.2	92.1	93.1	99.2	52.0	95.5	83.6	**99.8**
S8	55.7	91.2	87.7	98.3	85.0	87.6	95.0	99.3	80.5	91.7	93.6	**99.7**
S9	61.5	76.2	71.2	89.8	73.9	93.7	96.7	99.7	75.3	93.9	93.4	**99.8**
S10	61.7	88.7	81.0	94.2	92.1	99.1	99.1	99.5	67.5	92.9	82.4	**99.8**
S11	66.3	95.7	94.5	95.9	89.6	82.4	99.7	99.0	67.3	88.1	92.5	**99.1**
S12	63.1	84.3	77.4	82.6	63.8	90.6	91.3	98.3	62.6	86.1	77.6	**98.3**
S13	51.9	88.2	83.4	93.4	57.6	89.6	80.3	98.0	62.9	93.1	82.4	**99.2**
S14	69.5	98.4	97.3	98.7	58.9	91.9	95.7	99.3	52.4	96.7	94.8	**99.9**
Mean	63.4	88.1	84.5	93.6	75.9	88.8	94.1	96.7	65.9	90.7	85.7	**98.9**

(Best values found are in bold)

TABLE 7. Subject-wise testing accuracy was obtained using VMD, EWT, and VMD-EWT with four different classifiers- Naïve Bayes, SVM, LDA, and ensemble subspace KNN classifier with the 5-fold cross cross-validation technique for human activity prediction during sitting, standing, and walking.

Subject	VMD				EWT				VMD-EWT			
	NB	SVM	LDA	Ensemble Subspace KNN	NB	SVM	LDA	Ensemble Subspace KNN	NB	SVM	LDA	Ensemble Subspace KNN
S1	69.2	83.9	79.2	86.7	85.6	88.3	91.9	83.8	54.2	86.1	78.5	**96.5**
S2	68.9	87.4	87.4	89.1	84.6	88.9	94.9	81.2	52.8	92.9	80.0	**98.5**
S3	67.0	90.0	87.7	96.9	55.7	90.6	92.6	94.6	78.1	91.7	84.1	**99.8**
S4	53.1	78.6	81.0	93.1	78.3	86.5	96.1	98.3	84.2	89.2	93.2	**99.6**
S5	58.1	84.5	77.3	98.2	80.9	86.8	100	99.5	56.4	88.7	89.1	**98.1**
S6	70.7	93.8	91.2	93.8	75.4	88.0	94.9	99.8	82.6	92.3	87.5	**96.9**
S7	62.3	99.4	98.2	98.2	70.0	93.9	93.0	99.6	53.0	95.1	82.7	**99.8**
S8	56.4	92.2	88.7	98.5	88.6	91.5	97.7	99.3	77.4	90.7	92.1	**99.9**
S9	60.7	80.7	77.1	89.5	73.4	94.7	96.3	99.8	75.4	93.2	94.7	**100.0**
S10	65.4	88.6	80.5	94.7	92.8	99.4	99.4	99.2	65.7	93.6	80.2	**99.4**
S11	63.7	97.7	95.0	97.3	91.1	85.0	100	99.2	60.6	88.6	93.0	**99.7**
S12	65.0	84.9	74.1	84.9	58.1	92.4	90.8	97.1	63.0	87.7	79.0	**98.5**
S13	52.0	85.5	82.7	96.4	59.9	90.1	82.8	98.8	61.7	93.9	83.5	**99.3**
S14	70.9	98.8	97.6	98.6	59.9	92.2	91.7	99.6	51.9	97.2	94.7	**99.9**
Mean	63.1	89.0	85.5	93.9	75.3	90.5	94.4	96.4	65.5	91.4	86.5	**98.9**

(Best values found are in bold)

from noisy sEMG data. The discrimination strength of the obtained features was further increased by applying correlation coefficients and performing multiresolution analysis.

A. THE VMD FOR SEMG DECOMPOSITION

Composing sEMG signals using VMD represents a crucial preprocessing step in our study. FIGURE 8 vividly illustrates VMD's performance and effectiveness in decomposing

TABLE 8. Subject-wise testing performance measures with ensemble subspace KNN classifier during VMD-EWT.

Subject	Accuracy	Precision	F1-Score	Sensitivity
S1	96.5	96.5	96.8	97.2
S2	98.5	98.7	98.7	98.7
S3	99.8	99.5	99.6	99.7
S4	99.6	99.6	99.6	99.6
S5	98.1	98.2	97.5	96.9
S6	96.9	97.5	97.2	97.0
S7	99.8	99.7	99.7	99.7
S8	99.9	99.9	99.8	99.8
S9	100.0	100.0	100.0	100.0
S10	99.4	99.0	98.6	98.1
S11	99.7	99.4	99.5	99.7
S12	98.5	98.5	98.1	97.7
S13	99.3	99.0	99.0	98.9
S14	99.9	99.9	99.9	99.9
Mean	98.9	98.9	98.8	98.7

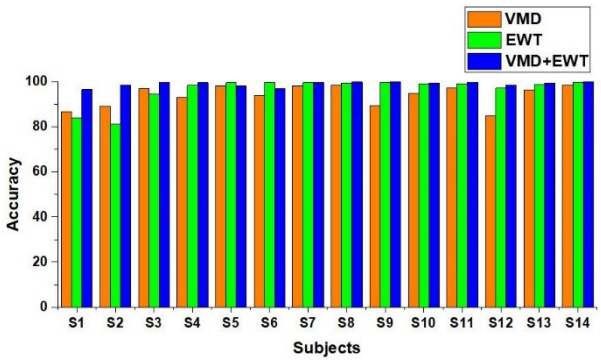

FIGURE 10. Comparison graph of VMD, EWT, and VMD-EWT.

sEMG signals into IMFs. This section discusses the essential findings and implications of our VMD decomposition results.

In FIGURE 8 illustrate the sEMG signal decomposed into multiple IMFs. Each IMF captures specific temporal and spectral characteristics of the original signal. This decomposition allows us to gain insights into the underlying physiological and biomechanical processes involved in muscle activation. The presence of distinct IMFs suggests that the sEMG signal comprises various frequency components, which can be attributed to motor unit recruitment, muscle fatigue, and other factors. VMD also facilitates the removal of noise and artifacts from the sEMG signal. This residual component can be analyzed to assess the decomposition's quality and identify and eliminate artifacts, thereby improving the reliability of subsequent analyses.

B. EWT ON SELECTED IMFS

The proposed work extended the signal decomposition process beyond VMD by applying the EWT to a subset of the IMFs obtained from VMD. The purpose was to enhance signal separability stability and extract more intricate characteristics from complex non-stationary sEMG signals, as seen in FIGURE 9. The results of this two-step decomposition process have significant implications, particularly in signal processing, which plays a vital role in signal detection, classification, and recognition. One of the notable outcomes of applying EWT to the selected IMFs from VMD is improved signal separability and stability.

EWT decomposes each selected IMF into a multiresolution analysis (MRA) set, which are adaptively constructed basis functions. This adaptability allows EWT to capture the fine-scale details of each IMF, leading to better separation of different signal components. Consequently, the processed IMFs exhibit enhanced clarity and distinctiveness of their underlying features, which are paramount for accurate signal analysis.

C. SUBJECT-WISE VALIDATION AND TESTING FOR DIFFERENT CLASSIFIERS- NAÏVE BAYES, SVM, LDA, AND ENSEMBLE SUBSPACE KNN CLASSIFIER

The proposed work systematically evaluated the performance of multiple classifiers, including Naïve Bayes, SVM, LDA, and the Ensemble Subspace KNN Classifier, using subject-wise validation to assess their effectiveness in classifying sEMG signals. The aim was to identify the classifier with the highest accuracy and reliability for this specific application. TABLE 6 summarises subject-wise validation of the accuracy obtained using VMD, EWT, and VMD-EWT. When the VMD method is applied to the same dataset, Mean accuracies obtained: NB-63.4%, SVM-88.1%, LDA-84.5%, and Ensemble Subspace KNN-93.6% without EWT. With EWT applied, mean accuracies

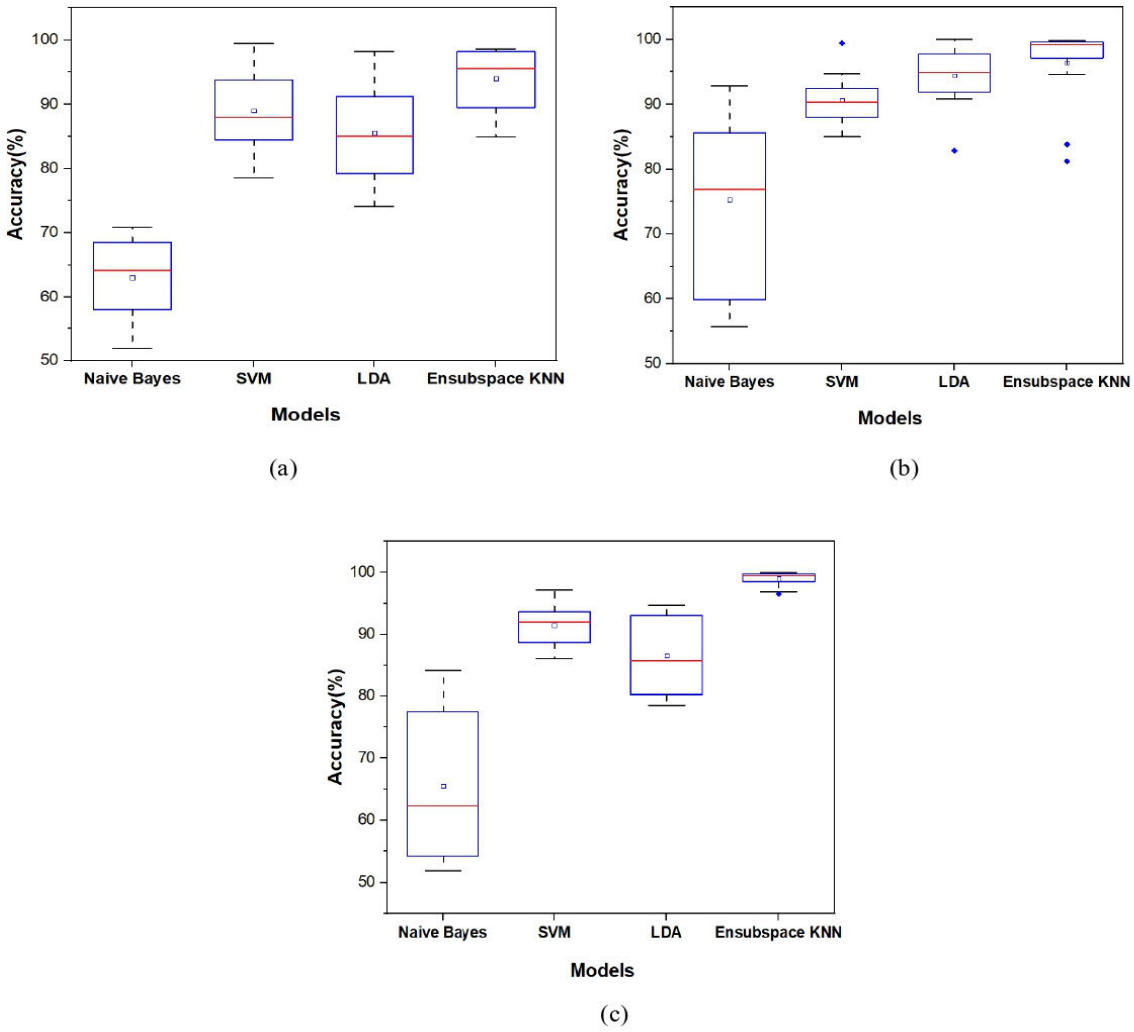

FIGURE 11. Box plot of the Classification model a)VMD b)EWT c)VMD-EWT.

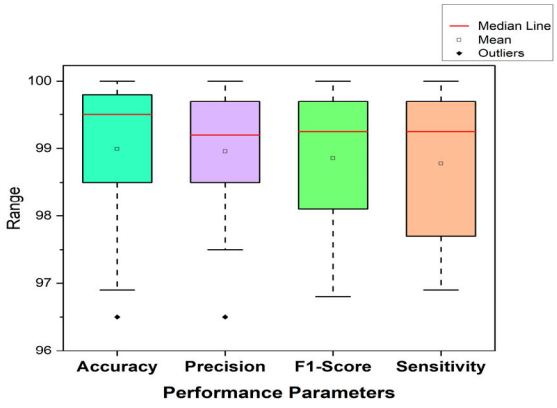

FIGURE 12. Box plot of performance parameter with VMD-EWT-Ensemble subspace KNN.

were NB-75.9%, SVM-88.8%, LDA-94.1%, and Ensemble Subspace KNN-96.7%. Finally, with VMD-EWT combined, mean accuracies reached NB-65.9%, SVM-90.7%, LDA-85.7%, and Ensemble Subspace KNN-98.9%.

TABLE 7 summarises subject-wise testing accuracy obtained using VMD, EWT, and VMD-EWT. When the VMD method is applied to the same dataset, mean accuracies obtained are NB-63.1%, SVM-89.0%, LDA-85.5%, and Ensemble Subspace KNN-93.9%. Applying EWT to the same dataset yields mean accuracies of NB-75.3%, SVM-90.5%, LDA-94.4%, and Ensemble Subspace KNN-96.4%. Finally, with the combination of VMD-EWT, mean accuracies are NB-65.5%, SVM-91.4%, LDA-86.5%, and Ensemble Subspace KNN-98.9%. Observing the results, it's evident that the Ensemble Subspace KNN model achieves the highest accuracy across VMD, EWT, and VMD-EWT methods, with the proposed VMD-EWT method reaching a particularly high mean accuracy of 98.9%.FIGURE 10 illustrates the comparison graph of VMD, EWT, and VMD-EWT with 14 subjects and their accuracy obtained, where the proposed model gives the highest accuracy.

FIGURE 11 illustrates that the VMD-EWT approach combined with the Ensemble Subspace KNN model exhibits a notably higher median accuracy compared to the VMD

TABLE 9. Comparison of several methods for classifying lower limb activity recognition and the accuracy that was attained.

Ref	Methods	Feature	Classifier	Dataset	Results
[24]	WT	Time Domain and Frequency Domain	SVM	Original EMG Dataset	4 Motions 91.85%
[34]	ICA-EBM	Time Domain	LDA	UCI	3 Motions 96.1% Normal 86.2% Abnormal
[35]	-	Time Domain	ANN	Other	2 Motions 87.4% Normal
[9]	End-End Transfer Learning	-	LRCN - MyoNet	UCI	3 Motions 92.4% Abnormal
[36]	WPT,PCA and SUKFNN	-	NN	Own Dataset	5 Motions 93.7%
[37]	WD-EEMD	Time Domain	LDA	UCI	3 Motions 90.69% Normal 97.45% Abnormal
[38]	PCA,LDA ,RPDA	-	NN	HAR-sEMG	5 Motions 90.22-PCA,81.8 - LDA,90.0 6-RPDA
[43]	FSA	Time Domain and Frequency Domain	NN	Own Dataset	5 Motions 97.73%
[39]	VMD	-	CNN-KELM	Other	5 Motions 95.90
[40]	VMD	Entropy Feature	NB	Other	4 Motions 97.44
[44]	SWRF	-	Random forests	Other	89.06
[45]	WPT	-	BPNN	Own Dataset	6 Motions 94.83
Proposed	VMD+EWT	Time Domain+Frequency Domain+Entropy	Ensemble Subspace KNN	Original EMG dataset	3 Motions 98.9

neural network (NN), wavelet packet transform (WPT), principal component analysis (PCA), Kalman filter (SUKF), Convolutional neural network with kernel extreme learning machine (CNN-KELM), independent component analysis (ICA), wavelet transform(WT), Wavelet denoising (WD) , Feature Selection Algorithm (FSA), stacked weighted random forest (SWRF)

and EWT approaches. This suggests that, on average, the VMD-EWT combined with the Ensemble Subspace KNN model offers superior accuracy in the given dataset or scenario. Utilizing a box plot to evaluate model performance enables a quick and informative comparison of different approaches, providing clear insights into their relative strengths and weaknesses. The box plot visually represents the distribution of accuracies, highlighting that the accuracy rate of the Ensemble Subspace KNN surpasses that of SVM, LDA, and Naïve Bayes. Additionally, the dispersion of the Ensemble Subspace KNN is observed to be smaller compared to SVM, LDA, and Naïve Bayes, indicating a more consistent performance across the dataset. The results emphasize the effectiveness of the combined VMD-EWT approach with the Ensemble Subspace KNN model in achieving higher accuracy, making it a promising choice for the given task or dataset. Further analysis and potentially additional statistical tests could be conducted to validate and quantify these observed differences in accuracy.

D. VMD-EWT METHODS PERFORMANCE MEASURES USING ENSEMBLE SUBSPACE KNN CLASSIFIER

The Proposed model is evaluated using an ensemble subspace KNN classifier based on performance measures like accuracy, precision, F1-score, and sensitivity. The subject-wise performance measures are obtained, with mean accuracy- 98.9%, precision- 98.9%, F1-score -98.8%, and sensitivity- 98.7%, as shown in TABLE 8.

FIGURE 12 provides box plots as a valuable visualization tool for gaining insights into the performance distribution of the Ensemble subspace KNN classification model. These box plots provide a clear and informative representation of key performance metrics, such as accuracy, precision, F1-score, and sensitivity for 14 subjects.

The proposed VMD-EWT method combines the highest accuracy with other existing models where [24] proposed WT method for activity prediction with SVM-91.85%, [35] worked on time-domain features and applied ANN for knee abnormality prediction. Reference [34] implemented the ICA-EBM method for motion detection with LDA-96.1% for normal and 86.2% for abnormal on the UCI dataset. Reference [9] proposed end-end transfer learning with LRCN-MyoNet-92.4%. Reference [36] worked on WPT, PCA, and SUKFNN and achieved 93.7% accuracy. Reference [37] implemented WD-EEMD with LDA-90.69%. Reference [38] worked on NN model for 5 motion prediction where PCA-90.2%,LDA-81.8% and RPDA-90.0% results are obtained. Reference [39] proposed VMD method with CNN-KELM-95.90%, [40] worked on VMD with Entropy Feature. The Proposed work is on VMD-EWT with a combined feature set of time-domain, frequency-domain, and entropy features obtained and achieved the highest accuracy, 98.9%, compared with the above state-of-art methods as given in TABLE 9.

V. CONCLUSION AND FUTURE SCOPE

In conclusion, the proposed preprocessing approach based on VMD and EWT presents a robust solution for classifying and analyzing sEMG signals, holding significant promise across various fields including kinesiological research, motion intention recognition, rehabilitation, human-machine interaction, and disease diagnosis. By effectively mitigating noise interference in sEMG signals through VMD and EWT, signal separability and stability are notably improved, particularly in capturing low-frequency components.

Our method demonstrates excellence in sEMG signal processing, employing EWT for IMF decomposition into MRA to facilitate feature extraction across time and frequency domains as well as entropy measures. With successful segmentation of signals and extraction of 16 key features, we evaluated four machine learning classifiers for lower limb

movement classification, with the Ensemble Subspace KNN classifier emerging as the top performer, achieving impressive results with high sensitivity, F1-Score, and accuracy.

Looking forward, future research avenues include validating our method with larger and more diverse datasets to enhance robustness and generalizability. Exploring real-time applications in clinical settings and investigating advanced feature engineering techniques and dimensionality reduction methods could further optimize the feature set. Additionally, exploring complex ensemble models and deep learning architectures holds promise for achieving even higher classification accuracy. Collaborations across interdisciplinary fields offer opportunities for innovative applications in areas such as prosthetics, assistive devices, and motor function assessment.

REFERENCES

[1] S. Ranasinghe, F. Al Machot, and H. C. Mayr, "A review on applications of activity recognition systems with regard to performance and evaluation," *Int. J. Distrib. Sensor Netw.*, vol. 12, no. 8, Aug. 2016, Art. no. 155014771666552, doi: 10.1177/1550147716665520.

[2] V. B. Semwal, N. Gaud, P. Lalwani, V. Bijalwan, and A. K. Alok, "Pattern identification of different human joints for different human walking styles using inertial measurement unit (IMU) sensor," *Artif. Intell. Rev.*, vol. 55, no. 2, pp. 1149–1169, Feb. 2022, doi: 10.1007/s10462-021-09979-x.

[3] G. J. Rani, M. F. Hashmi, and A. Gupta, "Surface electromyography and artificial intelligence for human activity recognition—A systematic review on methods, emerging trends applications, challenges, and future implementation," *IEEE Access*, vol. 11, pp. 105140–105169, 2023, doi: 10.1109/ACCESS.2023.3316509.

[4] Y. Sun, Y. Tang, J. Zheng, D. Dong, X. Chen, and L. Bai, "From sensing to control of lower limb exoskeleton: A systematic review," *Annu. Rev. Control*, vol. 53, pp. 83–96, Jan. 2022, doi: 10.1016/j.arcontrol.2022.04.003.

[5] R. Swaroop, M. Kaur, P. Suresh, and P. K. Sadhu, "Classification of myopathy and neuropathy EMG signals using neural network," in *Proc. Int. Conf. Circuit,Power Comput. Technol. (ICCPCT)*, Apr. 2017, pp. 1–5, doi: 10.1109/ICCPCT.2017.8074330.

[6] K. Rezaee, S. Savarkar, X. Yu, and J. Zhang, "A hybrid deep transfer learning-based approach for Parkinson's disease classification in surface electromyography signals," *Biomed. Signal Process. Control*, vol. 71, Jan. 2022, Art. no. 103161, doi: 10.1016/j.bspc.2021.103161.

[7] P. K. Shukla, A. Vijayvargiya, and R. Kumar, "Human activity recognition using accelerometer and gyroscope data from smartphones," in *Proc. Int. Conf. Emerg. Trends Commun., Control Comput. (ICONC)*, Feb. 2020, pp. 1–6, doi: 10.1109/ICONC345789.2020.9117456.

[8] A. Vijayvargiya, C. Prakash, R. Kumar, S. Bansal, and J. M. R. S. Tavares, "Human knee abnormality detection from imbalanced sEMG data," *Biomed. Signal Process. Control*, vol. 66, Apr. 2021, Art. no. 102406, doi: 10.1016/j.bspc.2021.102406.

[9] A. Gautam, M. Panwar, D. Biswas, and A. Acharyya, "MyoNet: A transfer-learning-based LRCN for lower limb movement recognition and knee joint angle prediction for remote monitoring of rehabilitation progress from sEMG," *IEEE J. Transl. Eng. Health Med.*, vol. 8, pp. 1–10, 2020, doi: 10.1109/JTEHM.2020.2972523.

[10] N. Nazmi, M. A. Rahman, S.-I. Yamamoto, S. Ahmad, H. Zamzuri, and S. Mazlan, "A review of classification techniques of EMG signals during isotonic and isometric contractions," *Sensors*, vol. 16, no. 8, p. 1304, Aug. 17, 2016, doi: 10.3390/s16081304.

[11] A. L. Ricamato, R. G. Absher, M. T. Moffroid, and J. P. Tranowski, "A time-frequency approach to evaluate electromyographic recordings," in *Proc. Symp. Comput.-Based Med. Syst.*, Jun. 1992, pp. 520–527, doi: 10.1109/CBMS.1992.245010.

[12] N. E. Huang, Z. Shen, S. R. Long, M. C. Wu, H. H. Shih, Q. Zheng, N.-C. Yen, C. C. Tung, and H. H. Liu, "The empirical mode decomposition and the Hilbert spectrum for nonlinear and non-stationary time series analysis," *Proc. Roy. Soc. London. Ser. A: Math., Phys. Eng. Sci.*, vol. 454, no. 1971, pp. 903–995, Mar. 1998.

[13] H. Ge, G. Chen, H. Yu, H. Chen, and F. An, "Theoretical analysis of empirical mode decomposition," *Symmetry*, vol. 10, no. 11, p. 623, Nov. 2018, doi: 10.3390/sym10110623.

[14] H. Ashraf, U. Shafiq, Q. Sajjad, A. Waris, O. Gilani, M. Boutaayamou, and O. Brüls, "Variational mode decomposition for surface and intramuscular EMG signal denoising," *Biomed. Signal Process. Control*, vol. 82, Apr. 2023, Art. no. 104560, doi: 10.1016/j.bspc.2022.104560.

[15] P. L. Singh, S. M. Verma, A. Vijayvargiya, and R. Kumar, "WD-EEMD based voting classifier for hand gestures classification using sEMG signals," in *Proc. IEEE 6th Int. Conf. Comput., Commun. Autom. (ICCCA)*, Dec. 2021, pp. 225–230, doi: 10.1109/ICCCA52192.2021.9666291.

[16] A. A. Mousavi, C. Zhang, S. F. Masri, and G. Gholipour, "Structural damage detection method based on the complete ensemble empirical mode decomposition with adaptive noise: A model steel truss bridge case study," *Struct. Health Monitor.*, vol. 21, no. 3, pp. 887–912, May 2022, doi: 10.1177/14759217211013535.

[17] Y. Li, N. Zhu, and Y. Hou, "Comparison of empirical modal decomposition class techniques applied in noise cancellation for building heating consumption prediction based on time-frequency analysis," *Energy Buildings*, vol. 284, Apr. 2023, Art. no. 112853, doi: 10.1016/j.enbuild.2023.112853.

[18] G. Lu, J.-S. Brittain, P. Holland, J. Yianni, A. L. Green, J. F. Stein, T. Z. Aziz, and S. Wang, "Removing ECG noise from surface EMG signals using adaptive filtering," *Neurosci. Lett.*, vol. 462, no. 1, pp. 14–19, Sep. 2009, doi: 10.1016/j.neulet.2009.06.063.

[19] K. Dragomiretskiy and D. Zosso, "Variational mode decomposition," *IEEE Trans. Signal Process.*, vol. 62, no. 3, pp. 531–544, Feb. 2014, doi: 10.1109/TSP.2013.2288675.

[20] S. Lahmiri and M. Boukadoum, "Biomedical image denoising using variational mode decomposition," in *Proc. IEEE Biomed. Circuits Syst. Conf. (BioCAS)*, Oct. 2014, pp. 340–343, doi: 10.1109/BIOCAS.2014.6981732.

[21] J. Gilles, "Empirical wavelet transform," *IEEE Trans. Signal Process.*, vol. 61, no. 16, pp. 3999–4010, Aug. 2013, doi: 10.1109/TSP.2013.2265222.

[22] W. Deng, S. Zhang, H. Zhao, and X. Yang, "A novel fault diagnosis method based on integrating empirical wavelet transform and fuzzy entropy for motor bearing," *IEEE Access*, vol. 6, pp. 35042–35056, 2018, doi: 10.1109/ACCESS.2018.2834540.

[23] Y. Song, S. Zeng, J. Ma, and J. Guo, "A fault diagnosis method for roller bearing based on empirical wavelet transform decomposition with adaptive empirical mode segmentation," *Measurement*, vol. 117, pp. 266–276, Mar. 2018, doi: 10.1016/j.measurement.2017.12.029.

[24] Y. Zhang, P. Li, X. Zhu, S. W. Su, Q. Guo, P. Xu, and D. Yao, "Extracting time-frequency feature of single-channel vastus medialis EMG signals for knee exercise pattern recognition," *PLoS ONE*, vol. 12, no. 7, Jul. 2017, Art. no. e0180526, doi: 10.1371/journal.pone.0180526.

[25] L. Dela, D. Sutopo, S. Kurniawan, T. Tjahjowidodo, and W. Caesarendra, "EMG based classification of hand gesture using PCA and SVM," in *Proc. 2nd Int. Conf. Electron., Biomed. Eng., Health Inform.*, 2022, pp. 459–477, doi: 10.1007/978-981-19-1804-9_35.

[26] S. Cai, D. Chen, B. Fan, M. Du, G. Bao, and G. Li, "Gait phases recognition based on lower limb sEMG signals using LDA-PSO-LSTM algorithm," *Biomed. Signal Process. Control*, vol. 80, Feb. 2023, Art. no. 104272, doi: 10.1016/j.bspc.2022.104272.

[27] R. S. Walse, G. D. Kurundkar, S. D. Khamitkar, A. A. Muley, P. U. Bhalchandra, and S. N. Lokhande, "Effective use of naïVe Bayes, decision tree, and random forest techniques for analysis of chronic kidney disease," in *Information and Communication Technology for Intelligent Systems*. Singapore: Springer, 2021, doi: 10.1007/978-981-15-7078-0_22.

[28] K. S. V. Swarna, A. Vinayagam, M. Belsam Jeba Ananth, P. Venkatesh Kumar, V. Veerasamy, and P. Radhakrishnan, "A KNN based random subspace ensemble classifier for detection and discrimination of high impedance fault in PV integrated power network," *Measurement*, vol. 187, Jan. 2022, Art. no. 110333, doi: 10.1016/j.measurement.2021.110333.

[29] W. Zhang, T. Zhao, J. Zhang, and Y. Wang, "LST-EMG-Net: Long short-term transformer feature fusion network for sEMG gesture recognition," *Frontiers Neurorobotics*, vol. 17, Feb. 2023, Art. no. 1127338, doi: 10.3389/fnbot.2023.1127338.

[30] R. T. Rockafellar, "A dual approach to solving nonlinear programming problems by unconstrained optimization," *Math. Program.*, vol. 5, no. 1, pp. 354–373, Dec. 1973, doi: 10.1007/bf01580138.

[31] L. Wen, J. Xu, D. Li, X. Pei, and J. Wang, "Continuous estimation of upper limb joint angle from sEMG based on multiple decomposition feature and BiLSTM network," *Biomed. Signal Process. Control*, vol. 80, Feb. 2023, Art. no. 104303, doi: 10.1016/j.bspc.2022.104303.

[32] A. Vijayvargiya, B. Singh, R. Kumar, and J. M. R. S. Tavares, "Human lower limb activity recognition techniques, databases, challenges and its applications using sEMG signal: An overview," *Biomed. Eng. Lett.*, vol. 12, no. 4, pp. 343–358, Nov. 2022, doi: 10.1007/s13534-022-00236-w.

[33] L. Pelaez Murciego, M. C. Henrich, E. G. Spaich, and S. Dosen, "Reducing the number of EMG electrodes during online hand gesture classification with changing wrist positions," *J. NeuroEng. Rehabil.*, vol. 19, no. 1, p. 78, Dec. 2022, doi: 10.1186/s12984-022-01056-w.

[34] G. R. Naik, S. E. Selvan, S. P. Arjunan, A. Acharyya, D. K. Kumar, A. Ramanujam, and H. T. Nguyen, "An ICA-EBM-based sEMG classifier for recognizing lower limb movements in individuals with and without Knee pathology," *IEEE Trans. Neural Syst. Rehabil. Eng.*, vol. 26, no. 3, pp. 675–686, Mar. 2018, doi: 10.1109/TNSRE.2018.2796070.

[35] N. Nazmi, M. A. A. Rahman, S.-I. Yamamoto, and S. A. Ahmad, "Walking gait event detection based on electromyography signals using artificial neural network," *Biomed. Signal Process. Control*, vol. 47, pp. 334–343, Jan. 2019, doi: 10.1016/j.bspc.2018.08.030.

[36] X. Shi, P. Qin, J. Zhu, M. Zhai, and W. Shi, "Feature extraction and classification of lower limb motion based on sEMG signals," *IEEE Access*, vol. 8, pp. 132882–132892, 2020, doi: 10.1109/ACCESS.2020.3008901.

[37] A. Vijayvargiya, B. Singh, R. Kumar, U. Desai, and J. Hemanth, "Hybrid deep learning approaches for sEMG signal-based lower limb activity recognition," *Math. Problems Eng.*, vol. 2022, pp. 1–12, Nov. 2022, doi: 10.1155/2022/3321810.

[38] Y. Luan, Y. Shi, W. Wu, Z. Liu, H. Chang, and J. Cheng, "HAR-sEMG: A dataset for human activity recognition on lower-limb sEMG," *Knowl. Inf. Syst.*, vol. 63, no. 10, pp. 2791–2814, Oct. 2021, doi: 10.1007/s10115-021-01598-w.

[39] J. Tu, Z. Dai, X. Zhao, and Z. Huang, "Lower limb motion recognition based on surface electromyography," *Biomed. Signal Process. Control*, vol. 81, Mar. 2023, Art. no. 104443, doi: 10.1016/j.bspc.2022.104443.

[40] C. Wei, H. Wang, F. Hu, B. Zhou, N. Feng, Y. Lu, H. Tang, and X. Jia, "Single-channel surface electromyography signal classification with variational mode decomposition and entropy feature for lower limb movements recognition," *Biomed. Signal Process. Control*, vol. 74, Apr. 2022, Art. no. 103487, doi: 10.1016/j.bspc.2022.103487.

[41] Y. Li, C. Zhang, and Y. Zhou, "A novel denoising method for ship-radiated noise," *J. Mar. Sci. Eng.*, vol. 11, no. 9, p. 1730, Sep. 2023.

[42] D. A. da Silva, N. F. L. C. Branco, L. S. de Andrade Mesquita, H. M. G. C. Branco, and G. de Alencar Barreto, "Electromyography and dynamometry in the prediction of risk of falls in the elderly using machine learning tools," *Biomed. Signal Process. Control*, vol. 88, Feb. 2024, Art. no. 105635.

[43] R. Gupta, I. S. Dhindsa, and R. Agarwal, "Surface electromyogram feature set optimization for lower limb activity classification," *IETE J. Res.*, vol. 69, no. 8, pp. 5000–5014, Sep. 2023.

[44] C. Shen, Z. Pei, W. Chen, J. Wang, X. Wu, and J. Chen, "Lower limb activity recognition based on sEMG using stacked weighted random forest," *IEEE Trans. Neural Syst. Rehabil. Eng.*, vol. 32, pp. 166–177, 2024, doi: 10.1109/TNSRE.2023.3346462.

[45] X. Shi, P. Qin, J. Zhu, S. Xu, and W. Shi, "Lower limb motion recognition method based on improved wavelet packet transform and unscented Kalman neural network," *Math. Problems Eng.*, vol. 2020, pp. 1–16, Apr. 2020.

[46] M. Grobbelaar, S. Phadikar, E. Ghaderpour, A. F. Struck, N. Sinha, R. Ghosh, and M. Z. I. Ahmed, "A survey on denoising techniques of electroencephalogram signals using wavelet transform," *Signals*, vol. 3, no. 3, pp. 577–586, Aug. 2022, doi: 10.3390/signals3030035.

GUNDALA JHANSI RANI (Member, IEEE) received the B.Tech. degree in electronics and communication engineering from the Balaji Institute of Technology and Sciences (BITS), Narsampet, Warangal, affiliated to JNTUH, in 2014, and the M.Tech. degree in embedded systems from the Vaagdevi Engineering College, Warangal, in 2016. She is currently pursuing the Ph.D. degree with the National Institute of Technology, Warangal, under the supervision of Dr. Md. Farukh Hashmi. Her primary areas of interests include EMG, the IoT, machine learning, and deep learning.

MOHAMMAD FARUKH HASHMI (Senior Member, IEEE) received the B.E. degree in electronics and communication engineering from MIT Mandsaur/RGPV Bhopal University, in 2007, the M.E. degree in digital techniques and instrumentation from the Shri Govindram Seksaria Institute of Technology and Science (SGSITS) (Autonomous State Government) Indore/RGPV Bhopal University, in 2010, and the Ph.D. degree from the Visvesvaraya National Institute of Technology (VNIT), Nagpur, in 2015, under the supervision of Dr. Avinash G. Keskar. He is an Assistant Professor with the Department of Electronics and Communication Engineering, National Institute of Technology (NIT), Warangal. He has a teaching and research experience of 13 years. He has supervised two Ph.D. scholars. He is currently guiding four Ph.D. scholars. He has published over 75 articles, including 25 SCI indexed research articles in international/national journals/conferences of publishers, such as IEEE, Elsevier, and Springer. He has also published one patent to his credit. He was a principal investigator of one research project of worth five Lakhs funded by the Institute Seed Grant through TEQIP III. His current research interests include computer vision, machine vision, machine learning, deep learning, embedded systems, the Internet of Things, digital signal processing, image processing, and digital IC design. He is a Life Member of IETE, ISTE, and IAENG. He is serving as an active and potential technical Reviewer for IEEE Access, *IET Image Processing*, *IET Computer Vision*, *Wireless Personal Communication*, IEEE Systems Journal, *Sensors* (MDPI), *Electronics* (MDPI), *Diagnostic* (MDPI), *The Visual Computer*, *Applied Soft Computing* (Elsevier), *Colour Research*, *The Journal of Super Computing*, and various other journals, such as Elsevier/Springer/IEEE Transactions publishers of repute.

GHULAM MUHAMMAD (Senior Member, IEEE) received the B.S. degree in computer science and engineering from Bangladesh University of Engineering and Technology, in 1997, and the M.S. and Ph.D. degrees in electronic and information engineering from Toyohashi University and Technology, Japan, in 2003 and 2006, respectively. He is a Professor with the Department of Computer Engineering, College of Computer and Information Sciences, King Saud University (KSU), Riyadh, Saudi Arabia. He has authored or coauthored more than 300 publications, including IEEE/ACM/Springer/Elsevier journals, and flagship conference papers. He owns two U.S. patents. He has supervised more than 15 Ph.D. and master's theses. He has involved in many research projects as a principal investigator and a co-principal investigator. His research interests include signal processing, machine learning, the IoT, medical signal and image analysis, AI, and biometrics. He was a recipient of the Japan Society for Promotion and Science (JSPS) Fellowship from the Ministry of Education, Culture, Sports, Science and Technology, Japan. He received the Best Faculty Award from Computer Engineering Department, KSU, from 2014 to 2015.